41st AIAA/ASME/SAE/ASEE Joint Propulsion Conference and Exhibit AIAA-2005-4250
July 10-13, 2005 – Tucson, Arizona

Discharge Chamber Plasma Structure of a 40-cm NEXT-type Ion Engine*

Daniel A. Herman† and Alec D. Gallimore.‡
Plasmadynamics and Electric Propulsion Laboratory
University of Michigan, Ann Arbor, MI 48109 USA

Langmuir probe plasma parameter data are presented over a two-dimensional array of spatial locations in the discharge chamber of a 40-cm diameter ring-cusp NEXT ion thruster. The discharge plasma structure is determined by the magnetic circuit, which reduces the diffusion of electrons across magnetic field lines. Number density profiles exhibit a highly collimated plume structure confined by the axial magnetic field near the discharge cathode assembly (DCA). A maximum value of $2x10^{13}$ cm^{-3} is measured along centerline at the keeper exit plane. A number density of ~$5x10^{11}$ cm^{-3} is observed outside of the discharge cathode plume. Electron temperatures in the cathode plume range from 2 – 4 eV increasing off-axis in the radial direction to 4 – 8 eV in the bulk discharge plasma. This increase is explained by electron acceleration across the free-standing potential gradient, termed a double layer, forming the transition between the discharge cathode plume and bulk discharge plasma. Between the magnetic cusps, near the anode, the electron temperature increases significantly. Only the high-energy electrons can cross the magnetic field lines to occupy these regions resulting in an increased electron temperature. Shorting of the discharge keeper to discharge cathode common, a condition of interest from ground-based NSTAR testing, does not have an effect on the near plasma structure outside of the DCA keeper sheath.

Nomenclature

A_p	=	electrode surface area, m^2
A_s	=	electrode sheath area, m^2
B	=	magnetic field magnitude, Gauss
c	=	effective exhaust velocity, km/s
g_0	=	gravity constant at sea level on earth, m/s^2
I_i	=	ion current to electrode, mA
$I_{i,\,sat}$	=	ion saturation current, mA
I_{sp}	=	specific impulse, s
J_a	=	acceleration grid current, mA
J_b	=	beam current, A
J_{dc}	=	discharge current, A
J_{nk}	=	neutralizer keeper current, A
k	=	Boltzmann's constant
K_n	=	Knudsen number
M_i	=	initial mass of spacecraft (including propellant), kg
M_f	=	final mass of spacecraft (dry mass), kg
M_{Xe}	=	mass of xenon ion, kg
$\dot{m}$	=	propellant mass flow rate, kg/s

* Color copies available at http://www.engin.umich.edu/dept/aero/spacelab/publications/conf_pub.html.

† Graduate Student, Aerospace Engineering, hermo@engin.umich.edu, 1919 Green Rd Room B107, Member AIAA.
‡ Professor and Laboratory Director, Aerospace Engineering, Alec.gallimore@umich.edu, Associate Fellow AIAA.

n = number density, cm^{-3}
n_e = electron number density, cm^{-3}
n_i = ion number density, cm^{-3}
P_b = base pressure (air), Torr
P_c = corrected pressure (xenon), Torr
P_i = indicated pressure (xenon), Torr
P_0 = discharge chamber pressure, Torr
q = electron charge, C
R_p = probe radius, m
T = thrust, N
T_{eV} = electron temperature, eV
V_a = acceleration grid voltage, V
V_b = electrode bias voltage with respect to discharge cathode, V
$V_{ck\text{-}cc}$ = keeper to cathode common voltage, V
V_{dc} = discharge voltage, V
V_g = coupling voltage, V
V_{nk} = neutralizer keeper voltage, V
V_s = screen grid voltage, V
Δv = velocity increment, km/s
ϕ = local plasma potential, V
λ = mean free path, m
λ_D = Debye length, m

I. Introduction

THE motivation for high exhaust velocity propulsion technology investment is illustrated by the Rocket Equation or Tsiolkovsky's Equation. Named after famous mathematics teacher Konstantin Tsiolkovsky, who in 1903 first published its derivation, the Rocket Equation identifies exhaust velocity as the important performance parameter in rocket propulsion.[1] The Rocket Equation illustrates that the fraction of the original vehicle mass that can be accelerated through a given velocity increment, Δv, is a negative exponential in the ratio of that velocity increment to the effective exhaust velocity, c.

$$\frac{M_f}{M_i} = e^{-\frac{\Delta v}{c}} = e^{-\frac{\Delta v}{I_{sp}\, g_0}} \tag{1}$$

As illustrated in Eq. 1, the effective exhaust velocity is related to the performance parameter specific impulse, Isp, which is defined as the total impulse per unit weight of propellant, given by Eq. 2.

$$I_{sp} \equiv \frac{T}{\dot{m} g_0} = \frac{c}{g_0} \tag{2}$$

Tsiolkovsky's Equation, Eq. 1, establishes the need for an effective exhaust velocity that is comparable with the mission Δv if a significant fraction of the original mass is to be brought to the final velocity. Deep space missions are prime examples of high-Δv missions that benefit from high exhaust velocity, but this can also be true for north-south station-keeping (NSSK) requirements in which long satellite lifetimes may require substantial Δv's to overcome the solar radiation pressure drag and gravity gradients to maintain their orbit. It is clear that there are many missions that can benefit from high exhaust velocity, or equivalently high specific impulse, technologies.

Ion thrusters are high-efficiency, high specific impulse (I_{sp}) propulsion systems that are being proposed as the primary propulsion source for a variety of missions. Ion thruster technology has enabled new missions that had not been feasible using liquid propellant rocket technology. The NASA Solar Electric Propulsion Technology Applications Readiness (NSTAR) 30-cm ion thruster was the first ion engine to be used for primary spacecraft propulsion in the Deep Space One (DS1) mission, validating ion thruster technology maturity for space flight. With

a design lifetime of 8,000 hours, the NSTAR ion thruster accumulated 16,265 hours of operation in space and the flight spare accumulated 30,352 hours of continuous operation in ground-based testing.[2,3]

A key component of the NSTAR program is ground-based testing of engineering model thrusters (EM's or EMT's) for extended periods of time. The first wear test of an engineering model 30-cm NSTAR thruster was the full-power (2.3-kW) 2000-hour wear test conducted at the NASA Glenn Research Center (GRC). The 2000-hour test, which did not employ a discharge cathode keeper, revealed extensive erosion of the two discharge cathodes used during the test.[4] Subsequent 1000-hour wear test and 8200-long duration test (LDT) employed a sacrificial keeper electrode demonstrating reduced discharge cathode erosion at an acceptable level (~60 μm/khr).[5-7] An Extended Life Test (ELT) of the NSTAR DS1 flight spare thruster, conducted at the Jet Propulsion Laboratory (JPL), revealed extensive keeper erosion that has yet to be fully explained. There is a lack of understanding of the discharge cathode assembly (DCA) erosion phenomena in ring-cusp ion thrusters. Engineering solutions, such as thicker keeper electrodes and more exotic keeper materials, may not be sufficient to achieve desired ion thruster lifetimes for future missions requiring several tens of thousands of hours.[8,9] A detailed understanding of the discharge plasma environment in ion thrusters will lead to better discharge designs and DCA erosion mitigation methods.

The successful demonstration of the NSTAR ion engine provides an off-the-shelf 2.3-kW ion engine suitable for discover class NASA missions. Several missions under consideration for the exploration of the Solar System have identified higher-power, higher-throughput 5/10-kW ion propulsion systems as a requirement for feasible missions.[10] For larger flagship-type missions, specifically robotic exploration of the outer planets using 25-kW-class solar-powered electric propulsion, NASA GRC has led a team to develop the next generation ion thruster. The 40-cm xenon ion engine, termed NASA's Evolutionary Xenon Ion Thruster (NEXT) was selected in 2002 for technology development as part of the Next Generation Electric Propulsion Project (NGEP).[11,12]

Several investigations have been underway to diagnose discharge cathode erosion in the 30-cm NSTAR ion thruster involving Laser-Induced Fluorescence (LIF) measurements, measurement of energetic ions near the DCA, and (concurrent with this investigation) electrostatic probing of the discharge chamber and discharge cathode.[13-20] High-resolution discharge plasma characterization of the near-DCA region of a 30-cm NSTAR thruster has been accomplished utilizing a high-speed probe positioning system.[21-24] Mapping the internal plasma structure of the 30-cm ion engine downstream of the DCA permitted the elimination of the potential hill theory as an explanation of the DCA erosion and illustrated a free-standing double layer plasma potential structure. The double layer is aligned with the axial magnetic field near the DCA and forms the transition between the low potential discharge cathode plume and the high potential bulk discharge plasma.

In an attempt to diagnose DCA erosion issues, an investigation of the discharge plasma structure of a 40-cm NEXT ion thruster has been initiated. To the author's knowledge this is the only internal investigation on a NEXT ion thruster to date. The purpose of this experiment is to obtain high spatial resolution plasma parameter measurements in the discharge chamber of the 40-cm NEXT ion engine, focusing on the near-DCA region. A secondary probe, located closer to the ion optics, offers additional valuable discharge chamber data. Determination of the discharge plasma environment permits evaluation of the DCA erosion mechanisms and estimation of the NEXT DCA erosion rate.[25]

II. 40-cm NEXT Ion Thruster

The NEXT ion engine follows the "derated" approach of the NSTAR program to preserve the NSTAR design heritage. This design approach maintains low beam current densities, low component operating temperatures (most importantly the permanent magnets), and reduces operating voltages that can accelerate wear mechanisms. To maintain low beam current densities while increasing throughput, an engine twice the beam area of the NSTAR thruster was designed. Increasing the engine beam diameter from 28-cm (NSTAR) to 40-cm (NEXT) doubles the beam extraction area. The higher beam area provides higher-power capability while maintaining comparable current densities, temperatures, and operating voltages. An input power of 4.7-kW on the NEXT engine operates at the same voltages and beam current density as 2.3-kW on the NSTAR engine. The NEXT engine can therefore be expected to yield the same operating lifetime while producing twice the thrust.

Figure 1. NEXT 40-cm engineering model ion thruster, courtesy of NASA.

A. NEXT Engine Design

The major components of the NEXT engine are designed based upon the NSTAR thruster. These include a non-ferrous spun-form discharge chamber, comparable discharge and neutralizer hollow cathode designs, similar electrical isolation techniques, analogous flake retention mesh, and dished two-grid ion-optics system. Improvements beyond NSTAR include: improved beam flatness via magnetic field design, a compact propellant isolator, increased beam voltage (up to 1800 V), and advanced ion optics design. The discharge and neutralizer cathodes have increased dimensions to accommodate the elevated current required along with some minor modifications. Performance testing of two engineering model thrusters and a laboratory model thruster exhibit peak specific impulse and thrust efficiency ranges of 4060 – 4090 seconds and 0.68 – 0.69, respectively, at the 6.1 kW power point.[26] A 2000 hour wear test has been conducted on Engineering Model 1 (EM1) at a thruster input power of 6.9 kW demonstrating specific impulse, thrust efficiency, and calculated thrust of 4110 s, 0.694, and 237 mN respectively.[27] A long-duration test of an EM thruster at NASA GRC has begun at the time of this publication and is expected to exceed 8000 hours of operation. At this date, the construction of a prototype model thruster is ongoing.[28]

B. Laboratory Model 4 (LM4) 40-cm NEXT Ion Thruster

The fourth-built, 40-cm laboratory model NEXT ion engine, referred to as LM4, was designed, fabricated, and assembled at NASA GRC. The engine design was modified with the intention of conducting electrostatic probe measurements and future Laser-Induced Fluorescence (LIF) measurements, inside the discharge chamber for normal engine operation *with beam extraction*. The LM4 variant is functionally equivalent to the NASA NEXT EM design with several incorporated features to facilitate discharge plasma interrogation and LIF characterization. The principal modifications between the LM4 and the EM thrusters include:

Figure 2. Laboratory model 4 (LM4) 40-cm NEXT ion thruster.

- Rotation of the gimbal and ion optics mounting by 45 degrees.
- Fabrication of a purely cylindrical plasma shield to facilitate access to the discharge chamber and reduce the complexity of the discharge plasma containment design.
- Anode fabrication from welded stainless steel sheet opposed to the NEXT EM thruster spun stainless steel anode.
- Incorporation of mechanical cathodes (employing machined Macor to isolate the cathode common, cathode heater, and cathode keeper) for the LM4 as opposed to the brazed cathode assemblies of the NEXT EM thrusters.
- Incorporation of a machined stainless steel optics mounting ring assembly instead of the ion optics stiffener ring mounting assembly of the EM's.
- Iso-mica optics spacer and macor tabs used to hold the grids in place and set the grid gap.
- Modification of the high-voltage propellant isolator design.
- Modification of the neutralizer mounting (at 45 degrees).

These design changes have a negligible effect on the operation of LM4 when compared to the 40-cm Engineering Model thrusters (EM's), as verified by magnetic field mappings and engine performance testing.[29]

C. LM4 Engine Modifications

Following confirmation of comparable performance to the EM's from characterization testing, the LM4 anode is modified for electrostatic probe access to the discharge chamber via slots in the side of the anode, shown in Figure 3. Slots are cut into the anode side and top for probe access and alignment of the probe to the discharge cathode assembly, respectively. Flanges are mounted to the slots permitting axial motion perpendicular to the flange opening and allowing easy transition between probe interrogation hardware and future LIF windows. The LM4 modifications and added hardware components are illustrated in Figure 3.

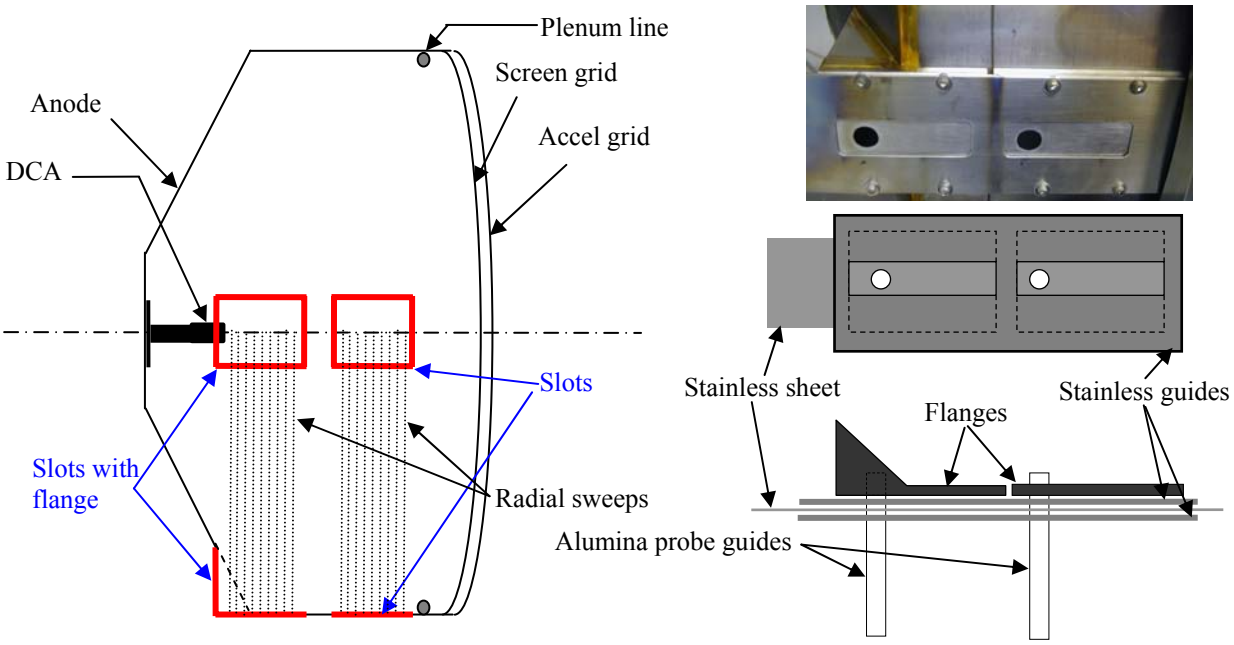

Figure 3. LM4 discharge interrogation modifications. Schematic of the slots and mounting flanges on anode (left). The discharge plasma containment hardware is illustrated on the right.

III. Experimental Apparatus

A. Vacuum Testing Facility

The LM4 discharge chamber investigations are conducted in the Plasmadynamics and Electric Propulsion Laboratory (PEPL) cylindrical 6-m-diameter by 9-m-long stainless steel-clad Large Vacuum Test Facility (LVTF). With seven cryopumps activated, surrounded by liquid nitrogen cooled baffles, the LVTF maximum pumping speed is 240,000 l/s on xenon (500,000 l/s on air). Pressure measurements, from a Varian model UHV-24 nude ion gauge with a Varian UHV senTorr vacuum gauge controller mounted on the LVTF wall, are corrected for xenon using the known base pressure on air, the indicated gauge pressure, and a correction factor of 2.87 for xenon according to,[30]

$$P_c = \frac{P_i - P_b}{2.87} + P_b . \tag{3}$$

The LVTF is operated with either four or seven cryopumps depending upon ion thruster operating condition. With four cryopumps, the facility pumping speed is 140,000 l/s on xenon with a base pressure typically $4\text{x}10^{-7}$ Torr. The LVTF can maintain a pressure in the low 10^{-6} Torr range during operation of the LM4 at low-to-mid power with the four cryopumps activated. To reduce the ingested flow into the discharge chamber, the LM4 testing is conducted with four cryopumps for low-to-mid power and with seven cryopumps for higher power. With seven cryopumps activated, the LVTF base pressure is $2\text{x}10^{-7}$ Torr. At the LM4 highest power condition permissible, the corrected background pressure is $2.8\text{x}10^{-6}$ Torr for a total xenon flow rate of 5 mg/s.

B. High-speed Probe Positioning System (HARP)

A linear motor assembly provides accurate direct linear motion of the probe with minimal discharge cathode plume residence times. The HARP system, shown in Figure 4, is a three-phase Trilogy 210 brushless dc servo motor consisting of a linear "U"-shaped magnet track and a "T"-shaped coil moving on a set of linear tracks. The linear encoder provides positioning resolution to 5 μm.[31] A Pacific Scientific SC950 digital, brushless servo drive controls the motor. The HARP is a linear table with a 559 mm stroke length. The HARP is capable of moving small probes at speeds above 250 cm/s with acceleration rates above 7 g's. The entire HARP table is enclosed in a stainless steel

shroud with a graphite outer skin. Residence times of the probe inside the discharge cathode plume are kept under 100 msec to minimize probe heating and discharge plasma perturbation. The HARP system was initially designed for internal discharge channel electrostatic probe measurements on Hall thrusters.[14,31-35] The HARP system is minimally modified for 30-cm NSTAR discharge chamber characterization and the near DCA 40-cm NEXT discharge plasma characterization.[21-24] The primary modifications include the probe mounting on-axis with the HARP and optimization of the control variables to achieve the desired sweep for trajectory given the HARP velocity and acceleration requirements.

Figure 4. High-speed Axial Reciprocating Probe (HARP) positioning system.

C. Axial Movement of Probe

A single-axis Aerotech ATS62150 linear ball screw translation table provides axial movement of the thruster relative to the probe. The Aerotech table has a travel length of 1.5 m with an accuracy of ±2.5 μm. A Renco RCM21 encoder provides precision measurement of the position of the thruster with a resolution of 5 μm and a frequency response of 200 kHz. The orientation of hardware and probes is illustrated in Figure 5. Two staggered electrostatic probes are inserted into the LM4 discharge plasma in the radial direction. The upstream probe characterizes the near-DCA region, while the downstream probe characterizes the near-optics region. The near-DCA mapping begins ~1.5 mm downstream of the discharge keeper face with an axial resolution of 1 mm. Each probe is activated individually, with the dormant probe floating. When actuated, the probe extends to the thruster centerline then returns to the starting location recessed inside the translating alumina tube. When not in use, the probes are recessed in the guiding alumina tube protecting the probes and reducing probe perturbations on the LM4 thruster operation.

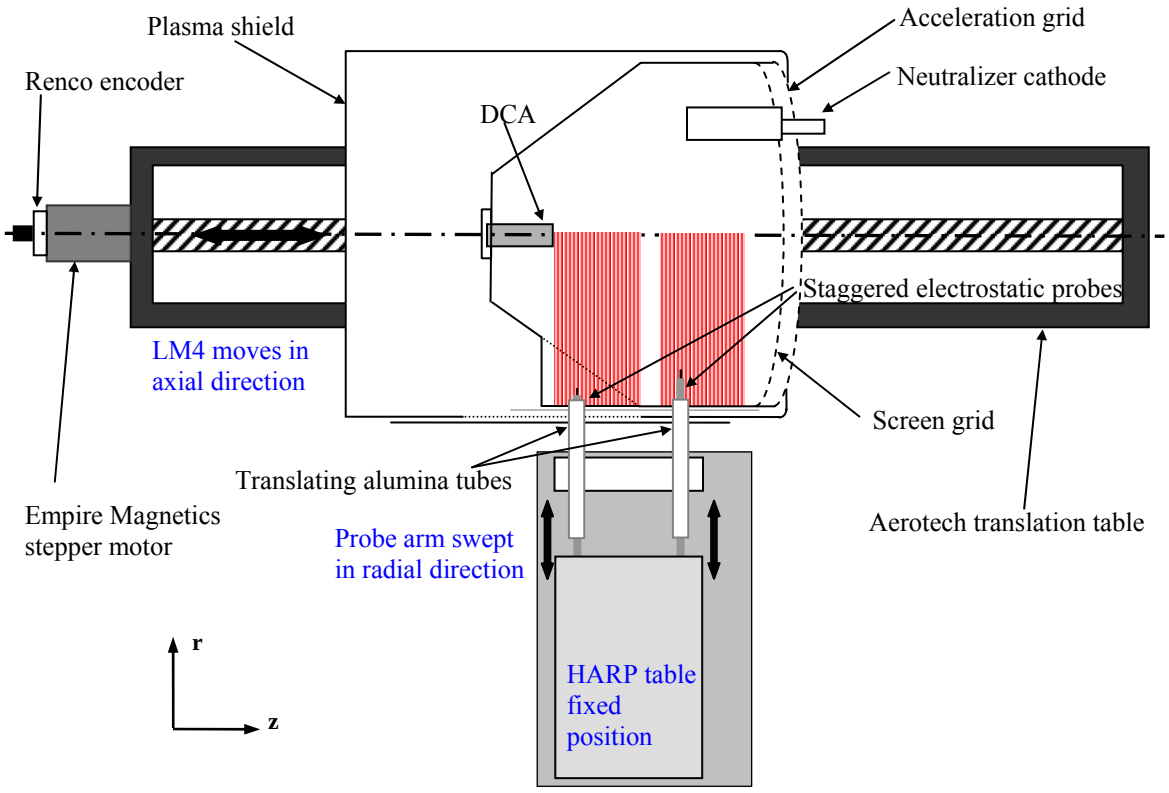

Figure 5. LM4 and HARP orientation with the translating table permitting axial movement.

IV. Langmuir Probe Diagnostic

Electrostatic probes have been extensively used to measure plasma parameters since their inception. Langmuir probes, named after the pioneering work performed by Irving Langmuir and collaborators, are one of the oldest and widely used probes in plasma characterization.[36,37] The single Langmuir probe consists of a single electrode connected to an external electrical circuit allowing variation of the probe voltage, V, with respect to the local plasma. Measurement of the probe bias voltage and collected current are plotted giving the current-voltage characteristic (I-V curve). The ease at which the data is taken, by biasing the probe with respect to another electrode (vacuum chamber, cathode common, anode, secondary electrode, etc…) and measuring the current to the probe, is offset by the difficulty in interpreting the resulting current-voltage (I-V) characteristic curve. The interpretation of the I-V curves is complicated by multiple regimes of operation, flowing plasma effects, and large magnetic fields. Appropriate analysis of the resulting "cold" electrostatic probe current-voltage (I-V) characteristic accurately provides multiple plasma parameters.

A. Theory of Operation

The single Langmuir probe theory is widely used and allows calculation of the fundamental local plasma parameters of interest, namely the number density and electron temperature. Langmuir probes measure local plasma parameters and are effectively shielded by the plasma particles when inserted into the plasma. Langmuir probe theory is divided into different probe regimes based upon two non-dimensional parameters: the Knudsen number (K_n) and Debye length (λ_D). The regime distinction between collisionless and continuum plasmas is related to the Knudsen number. The Knudsen number, defined in Eq. 4, relates the mean free path of charged particles to the probe radius. The mean free path of ions and electrons in the discharge chamber of ion engines is on the order of meters. This is larger than the physical dimensions of the discharge chamber and is much larger than the fraction of a millimeter sized probes used for this investigation. For $K_n >> 1$, a collisionless analysis is appropriate.

$$K_n \equiv \frac{\lambda}{R_p} \tag{4}$$

The ratio of the Debye length, given in Eq. 5, to probe radius determines the sheath analysis used. The electrostatic probes traverse two distinctly different plasmas inside the ion discharge resulting in two different sheath regime analysis techniques. Realistic electrode sizes of the single Langmuir probe, for the expected electron temperature (2 – 11 eV)[38,39] and number densities (10^{10} – 10^{12} cm^{-3}),[16,38] operate in the thin sheath regime near the discharge cathode. Inside the ion engine, the number densities are expected to have a maximum on cathode centerline and decrease by over two orders of magnitude with increasing radial distance from centerline driving an ever-increasing Debye length. The sheath width that forms around the probe is proportional to the Debye length and is therefore important to determine the probe operating regime. The relationship of the Debye length to electron number density and temperature is illustrated in Eq. 5:[40,41]

$$\lambda_D = 743\sqrt{\frac{T_{eV}}{n_e}} \tag{5}$$

The rapid growth in the Debye length with increasing radial distance from cathode centerline dictates that at some radial location inside the anode, the thin sheath criterion may not strictly apply. The Debye length is expected to grow to the same order of magnitude as the electrode radius in the bulk discharge plasma, indicating operation in the transition range between thin sheath and orbital motion limited (OML). In spatial locations near the anode, number densities are low enough for a complete OML analysis to be applicable.

B. Langmuir Probe Electrode

Several Langmuir probes are used due to breakage of probes caused by mechanical malfunction or user input error. All probes are slight variations on the basic probe design, illustrated in Figure 6. The basic design consists of 0.13 or 0.18-mm-diameter cylindrical tungsten electrode, with ~2 mm of exposed length. A large length to diameter ratio minimizes end effects. The electrode is held inside a double-bore tube of 99.8% pure alumina epoxied to a larger double-bore piece of 99.8% pure alumina. The ceramic probe material and tungsten filament are necessitated

by the high-temperature discharge plasma environment. The total length of the probe is approximately 0.5 m. After the probes are constructed, each is inspected under magnification to ensure cylindrical geometry. The probe tip electrodes are measured with a digital caliper and double checked under magnification.

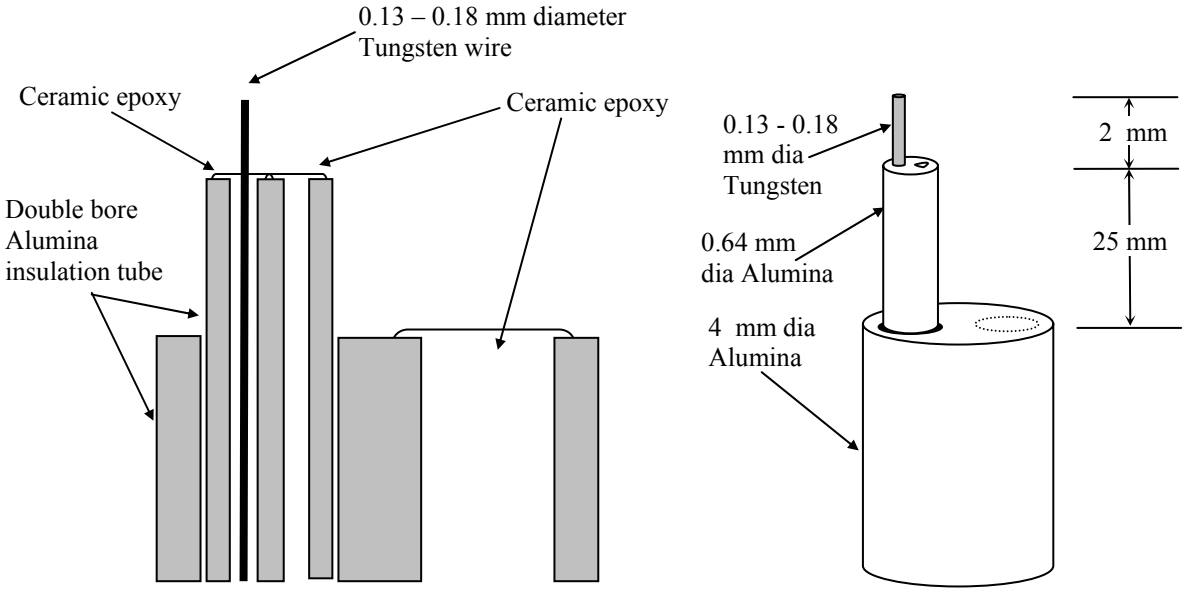

Figure 6: Langmuir probe tip design illustrating the components and physical dimensions.

C. Langmuir Probe Circuit

When the probe is swept into the discharge chamber, from a low-density plasma near the anode to a high-density discharge plasma plume, there is a rapid increase in plasma potential up to 1500 V for LM4. Significant errors in the measured current can occur due to any appreciable stray capacitance in the circuit. As such, careful attention is paid to minimizing stray capacitance in the circuit design including the use of batteries to supply the bias voltage. A potentiometer attached to the battery output sets the electrode bias voltage.

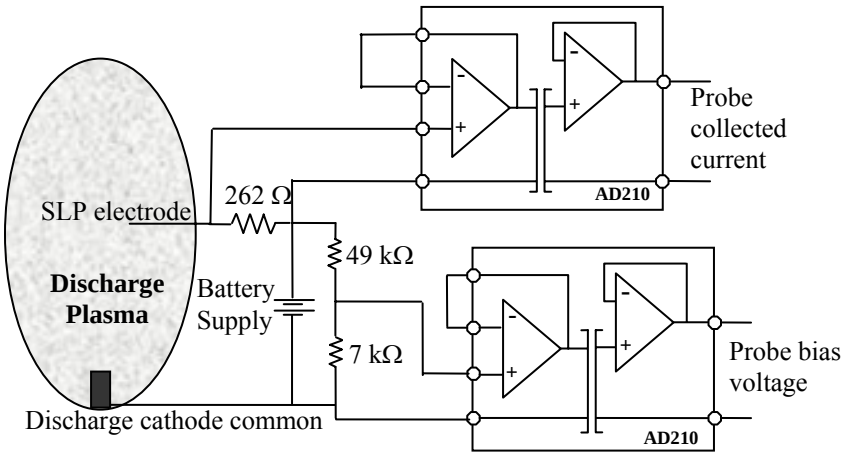

Figure 7: Single Langmuir probe circuit schematic.

The Langmuir probe circuit is built around two Analog Devices AD210 wide bandwidth isolation amplifiers, capable of handling up to 2500 volts of common mode voltage, providing an input impedance of 10^{12} Ω, and a full-power bandwidth of 20 kHz. The low-impedance output (1 Ω maximum) is connected to a Tektronix TDS 3034B digital oscilloscope that acquires the I-V data and saves it to a computer. Figure 7 illustrates the single Langmuir probe circuit. All connections extending outside the vacuum chamber are made using high-voltage (5 kV) SHV coaxial cables and feedthrus.

D. Langmuir Probe Data Analysis

The scientific graphing package Igor is used to analyze the data. The data are read into Igor, which reassembles the data into individual current-voltage (I-V) characteristics at discrete spatial locations in the two-dimensional grid illustrated in Figure 8. For each operating condition, I-V curves are obtained with a spatial resolution of 1 mm in both the axial and radial directions. The data collected for each operating condition incorporates 9,240 I-V traces for

each of the two probe domains in the LM4. The data analysis gives plasma parameters for all of these characteristics outputting contour images with a corresponding number of data points.

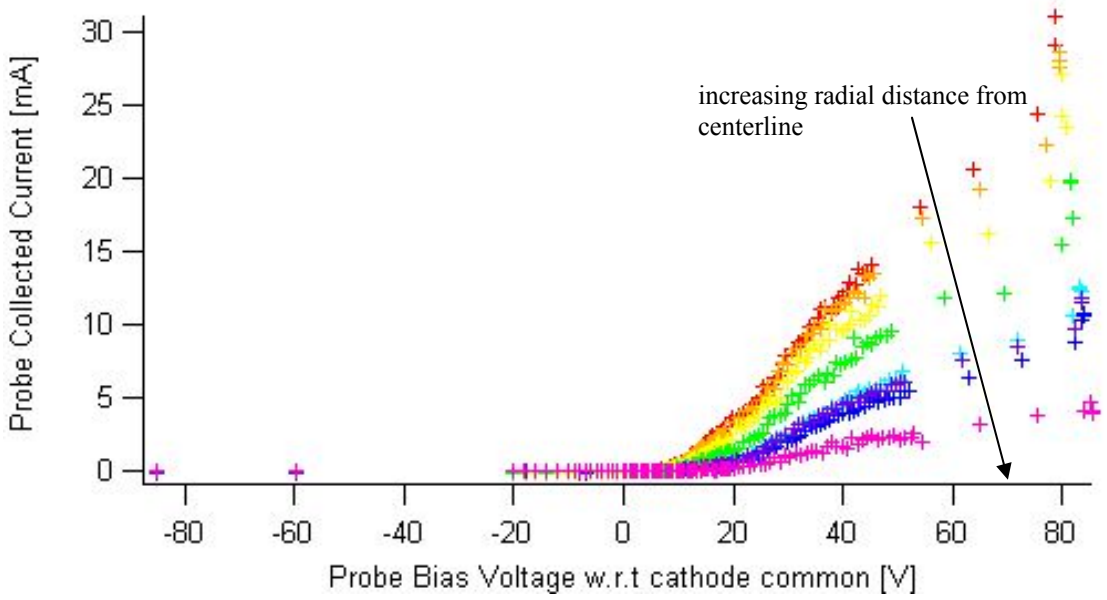

Figure 8: Sample current-voltage characteristics (I-V curves) reconstructed at specific spatial locations in the discharge chamber serving as the starting point for the Langmuir probe data analysis.

The relative sheath thickness compared to the probe radius is not known a priori; as a result, the data analysis code uses a multiple regime approach in the number density calculation. The individual Langmuir probe characteristics are analyzed, over the 2-D grid, assuming a purely Maxwellian electron population. The inverse slope of the natural log of the electron current versus voltage gives the Maxwellian electron temperature.

Near the DCA, the number density is high and a thin sheath analysis is warranted. A traditional thin sheath calculation is performed initially with the probe collection area equal to the electrode surface area. For a ratio of probe electrode radius to Debye length of greater than or equal to 10, a thin sheath analysis is applicable. The ion saturation current, the electron temperature, and the Bohm condition for ion velocity give the ion number density by Eq. 6.[36,40,41] The Bohm condition establishes that, for ion-attracting probes, electric fields in the quasi-neutral plasma exterior to the sheath (a pre-sheath) accelerate ions such that they enter the sheath with a velocity of $(kT_e/M_i)^{1/2}$. The Bohm velocity is the ion velocity necessary for a stable sheath. Assuming a quasi-neutral discharge plasma, the ion number density equals the electron number density:

$$n_{i,\,thin} = \frac{I_{i,\,sat}}{0.61\,A_s\,q}\sqrt{\frac{M_{Xe}}{k\,T_{eV}}}\,. \tag{6}$$

In Eq. 6, e is electron charge, M_{Xe} is the mass of the xenon ion, k is Boltzmann's constant, and A_s is the electrode collection area that is initially considered to be the electrode surface area. The true collection area depends upon the thickness of the sheath surrounding the probe. The actual sheath size is calculated based upon the measured plasma parameters. The probe collection area is increased including the sheath, resulting in a new number density. This iterative process continues until convergence. This procedure takes into account moderate departure from thin sheath.

Far from the DCA, a thick sheath exists and an orbital-motion-limited analysis is applicable. In the OML regime, ion orbits become important. Not all particles that enter the electrode sheath are collected. Particles can enter trapped orbits or enter and then exit the sheath. For a ratio of probe electrode radius to Debye length of less than or equal to 3, the electron temperature is still determined from the inverse slope of the natural log of the electron repelling

current versus bias voltage; however, the number density calculation must be made for an infinitely thick sheath. In the OML regime, the number density for cylindrical probes is calculated from the slope of the ion current squared versus bias voltage according to the following equation:[40,42,43]

$$n_{i,OML} = \sqrt{\frac{\left(-\Delta\left(I_i^2\right)/\Delta V_b\right)M_{Xe}}{0.2\,q^3\,A_p^2}}\ . \tag{7}$$

Between the two regimes, in the transition regime, a weighted average (based upon the ratio of Debye length to probe radius) is used to give smooth transition between the two regimes. The data analysis techniques used in this investigation can be found in References [40,42-48]. The large electron saturation currents near the DCA, which are not achievable with the given setup, preclude a plasma potential estimation in the DCA plume. Plasma potential mappings of the discharge plasma have been performed utilizing a floating emissive probe diagnostic in the LM4 thruster.[25,29]

E. Magnetic Field Effects

The magnetic field can affect Langmuir probe results by altering the I-V characteristic. The primary effect of the magnetic field is to confine electrons to spiral along the magnetic field lines and depress diffusion across the magnetic field line. As a result sheath structures around probes are no longer symmetric and can become oblong. The presence of a magnetic field has a negligible effect on the Langmuir probe measurements since the data analysis infers ion number density from the ion saturation current and therefore is unaffected by the reduction in electron saturation current caused by the presence of a magnetic field. The magnitude of the magnetic fields in ion thrusters is typically not large enough to have an appreciable effect on ion collection. However, the magnetic field can lead to electron energy distribution function (EEDF) anisotropy affecting the electron temperature measurement. Passoth determined that EEDF anisotropy depends upon the ratio B/p_o, where p_o is the pressure in the containment vessel (in this case the discharge chamber).[49] It has been shown experimentally that EEDF anisotropy is negligible for $B/p_o \leq 2.5\text{x}10^6$ G/Torr.[50]

The LM4 thruster has a maximum magnetic field (B), in the bulk discharge and near-DCA regions, occurring near the DCA along centerline. The maximum magnitude of the magnetic field in the near-DCA regions investigated is on the order of 100 G and the pressures in the discharge chambers of the engines are estimated to be $\sim 10^{-4}$ Torr. The LM4 measurements made near the cusps at the anode can reach magnetic field magnitudes on the order of a few hundred G. The value of B/p_o near the DCA is $1\text{x}10^6$, and for the worst case near the anode magnetic field cusps is $2\text{x}10^6$, therefore no substantial anisotropy in the EEDF is expected for the spatial locations interrogated.

The presence of the magnetic field results in a reduction of the electron saturation current, thereby affecting the plasma potential calculation from the I-V curves. Typically, the knee of the electron retarding region (or the maximum of the first derivative) is regarded as the local plasma potential. The magnetic field causes a shift in the calculated plasma potential resulting in a decrease in the magnitude calculated compared to the true plasma potential. This shift can be accounted for depending upon the orientation of the probe with the magnetic field, the electron temperature, and the mean free path of an electron.[51] The electron saturation current near the DCA is very large, sometimes several amps. The desire to minimize the discharge plasma perturbation, combined with the limitations of the battery supply and electrical circuit (in order to obtain better resolution), result in I-V characteristics that do not reach electron saturation. As a result, plasma potential calculations cannot be calculated from Langmuir probe data. Floating emissive probe testing performed on the LM4 thruster gives the plasma potentials for the same spatial domains.[25,29]

F. Error Analysis

Traditional estimates of the error in electrostatic probe measurements are 50% for electron number density and 20% for electron temperature.[42] While these absolute errors are large, the relative error between two measurements using identical setups is considerably smaller. Noise in measured electron temperatures near the anode is evident as the signal to noise ratio is greatly reduced by the reduction in number densities (and hence probe currents) at these spatial locations. Small DC offsets in the measured current, combined with the degraded signal-to-noise ratio, enhance the high electron temperatures in the near-anode region Near-anode electron temperature data are therefore given less confidence. A detailed investigation of the near anode plasma, with a modified circuit and a Langmuir probe tailored for the densities in this region, would permit a more accurate determination of electron temperature.

Number densities near the anode are relatively unaffected by the electron temperature fluctuations because the OML calculation, applicable in this region, is only a function of the slope of the ion saturation current. Comparisons of the data taken at equivalent thruster operating conditions indicate the excellent repeatability of the engine and electrostatic probe setup. The number density and electron temperature data, taken during different facility pump downs, illustrates comparable results for the near DCA and bulk discharge regions from two different probe tips.

G. Operating Conditions Investigated

The LM4 thruster Langmuir probe investigation is performed over a variety of thruster operating conditions limited at high-power by the beam and discharge power supplies. The investigation covers a range of conditions from low-to-mid power. In addition to the nominal operation with beam extraction, the thruster is operated with discharge-only (no beam extraction) and with the discharge keeper shorted to discharge cathode common. The LM4 operating conditions are labeled as single Langmuir probe (SLP) nominal Thruster Operating Conditions (TOC Levels), Discharge-only Levels (DL), and reference NEXT self-assigned Throttling Levels (TH Levels).

Table 1: Experiment LM4 single Langmuir probe (SLP) nominal Thruster Operating Conditions (TOC Levels) , Discharge-only Level (DL), and reference NEXT self-assigned Throttling Levels (TH Levels).

	TH	Vs	Jb	Va	Ja	Vdc	Jdc	Vnk	Jnk	Main Flow	D.C. Flow	Neut Flow	Vck-cc	Vg	Pressure
	Level	[v]	[A]	[V]	[mA]	[V]	[A]	[V]	[A]	[sccm]	[sccm]	[sccm]	[V]	[V]	[Torr]
~3800 seconds	TH 34	1567	3.10	-210.0	10.50	-	17.68	-	3.00	43.47	4.54	4.01	-	-	-
	SLP TOC 34'	1459	3.10	-210.1	7.90	23.84	16.64	12.85	3.00	42.5	4.54	4.0	3.65	-11.72	2.8E-06
	SLP TOC 34' CK-CC shorted	1455	3.10	-210.1	7.68	23.86	16.63	12.91	3.00	42.5	4.54	4.0	0.00	-11.70	2.8E-06
	SLP DL 34'	-	-	-	0.08	20.77	16.70	15.47	3.00	42.5	4.54	4.0	5.61	-0.80	2.8E-06
	TH 20	1567	2.00	-210.0	6.80	-	14.12	-	3.00	25.79	3.87	2.50	-	-	-
	SLP TOC 20'	1465	2.01	-210.0	9.15	24.87	13.45	13.86	3.00	24.5	3.87	2.5	0.76	-11.23	3.2E-06
~3300 seconds	TH 32	1179	3.10	-200.0	10.50	-	18.63	-	3.00	43.47	4.54	4.01	-	-	-
	SLP TOC 32	1179	3.10	-200.0	7.39	24.15	17.30	12.74	3.00	42.5	4.54	4.0	3.66	-11.51	2.8E-06
	TH 18	1179	2.00	-200.0	6.80	-	14.72	-	3.00	25.79	3.87	2.50	-	-	-
	SLP TOC 18	1179	2.01	-200.0	10.09	25.07	13.69	13.85	3.00	25.0	3.87	2.5	1.41	-11.45	3.2E-06
	TH 8	1179	1.20	-200.0	4.10	-	8.83	-	3.00	14.23	3.57	3.00	-	-	-
	SLP TOC 8	1179	1.20	-200.0	4.77	25.93	8.67	13.80	3.00	15.4	3.57	3.0	2.87	-10.20	2.4E-06
	SLP TOC 8 CK-CC shorted	1179	1.20	-200.1	4.82	26.09	8.68	14.00	3.00	15.4	3.57	3.0	0.00	-10.50	2.4E-06
	SLP DL 8	-	-	-	3.20	23.26	8.65	19.70	3.00	15.4	3.57	3.0	7.47	-0.85	2.2E-06
Low Power	TH 3	650	1.20	-144.0	4.10	-	9.54	-	3.00	14.23	3.57	3.00	-	-	-
	SLP TOC 3	649	1.20	-144.0	4.69	26.36	9.28	13.78	3.00	15.6	3.69	3.0	3.97	-9.98	2.4E-06
	TH 0	275	1.00	-500.0	3.40	-	7.99	-	3.00	12.32	3.52	3.00	-	-	-
	SLP TOC 0a	275	1.00	-500.0	3.45	26.15	7.71	14.34	3.00	13.9	3.59	3.0	5.62	-10.28	2.2E-06
	SLP TOC 0b	275	1.00	-500.0	16.82	26.32	7.72	14.85	3.00	13.3	3.59	3.0	3.88	-10.31	1.3E-06

V. Results

Detailed plasma parameter (number densities and electron temperatures) mappings are presented over a range of operating conditions on the LM4 thruster. Each contour plot contains 9,240 data points for each of the two interrogation regions (18,480 data points combined). The magnetic field streamlines, measured after the LM4 construction, are included in the parameter mappings to assist in their interpretation. Occasional radial streaks of anomalous electron temperature or number density are results of engine recycle events (momentary shorting between ion optic grids) during a radial sweep affecting the probe current collection.

A. Bulk Discharge Chamber Number Density Contours

A very distinct discharge cathode plume is evident from the number density contours in Figures 9 - 11. Inside the discharge cathode plume, number densities near the cathode exit approach $2x10^{13}$ cm^{-3} along centerline. The number densities decrease by an order of magnitude outside of the plume, at a distance on the order of the discharge keeper radius. The bulk discharge plasma density mappings are very similar over the range of operating conditions investigated with values ranging from $1x10^{11}$ to $1x10^{12}$ cm^{-3} in the bulk discharge. The thruster conditions span the

low power (V_s=275V, J_b=1.00A) settings to medium power (V_s=1500V, J_b=3.10A) settings. Just outside of the high-density cathode plume, the number densities are ~$5x10^{11}$ cm^{-3}, which is comparable to the value found in the 30-cm NSTAR thruster investigation.[23] This value is used, in conjunction with emissive probe plasma potential measurements to calculate a NEXT engine DCA erosion rate.[25,29]

The contour shapes, for the various operating conditions, are all identical and closely follow the magnetic field structure. Near the DCA, the magnetic field streamlines run almost entirely in the axial direction. This effectively confines the electrons emitted from the DCA to a narrow plume. These electrons spiral around the magnetic field lines resulting in ion creation in this narrow plume due to electron bombardment. The number densities near the anode cusp regions are larger in magnitude than the inter-cups regions where electrons are prevented from reaching due to the magnetic field.

Comparison of the number density contours in Figures 9 - 11 illustrates the following trends as the engine is throttled to higher power. In general there no discernable change in discharge plasma number density, outside of the DCA plume, as the thruster is operated at higher power levels. Slight variations are evident in the inter-cusp near-anode number densities, but are difficult to correlate to engine operating condition. A very modest decrease in the near-anode inter-cusp region is evident from low-power to medium-power settings. This may be due to the preferential drift of the ions towards the screen grid as the screen voltage and accelerator grid voltage are increased in magnitude. Essentially, the engine is more efficient at extraction of ions at the higher power setting. This is consistent with the decrease in discharge losses (W/A) measured for the NEXT ion engine with increasing thruster input power. This trend is attributed to the decreasing screen grid ion transparency associated with the decreasing total voltage (i.e. the sum of the magnitudes of the screen and accelerator grid voltages).

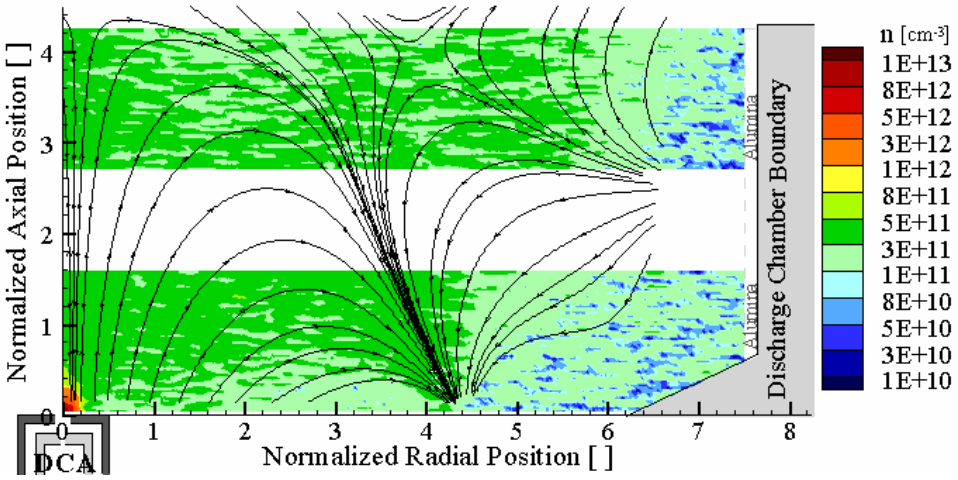

Figure 9: LM4 SLP TOC 0a (V_s = 275V and J_b = 1.00A) number density staggered probe results.

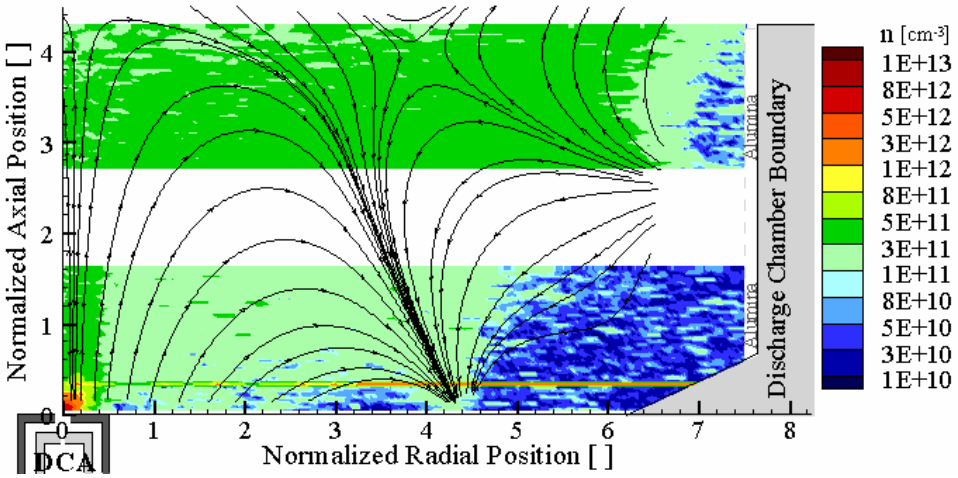

Figure 10: LM4 SLP TOC 8 (V_s = 1179V and J_b = 1.20A) number density staggered probe results.

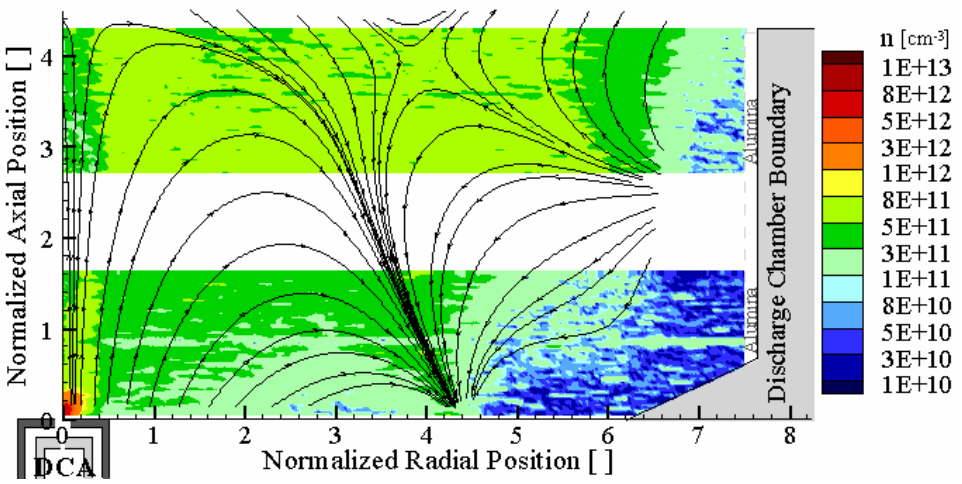

Figure 11: LM4 SLP Toc 34' (V_s = 1459V and J_b = 3.10A) number density staggered probe results.

Previous 30-cm ion thruster testing indicated that shorting the discharge cathode keeper to discharge cathode common had no effect outside of the keeper sheath.[22,23] This conclusion is supported by the LM4 results which illustrate negligible differences in the plasma structure when the keeper is shorted to common. The lack of beam extraction results in a slight decrease in number densities.

B. Bulk Discharge Electron Temperature Contours

Analysis of the single Langmuir probe results gives the electron temperature from the slope of the natural log of the I-V curve in the electron retarding region. This analysis is independent of the thin-sheath, thick-sheath, or transitional probe regime used. The electron temperature contours illustrate a discharge cathode plume where low electron temperatures exist (2 – 4 eV). Outside of this plume, the electron temperature gradually increases by a few volts to the bulk discharge electron temperatures of 4 to 7 eV. Near the anode, in the inter-cusp regions, the electron temperature reaches much higher values (as high as 13 – 15 eV). The near-anode rise in electron temperature may be enhanced by the reduced signal-to-noise ratio in this region. Sheath structures near the anode and/or the guiding alumina tube may affect the rising electron temperature measured. The electron temperature assumes a Maxwellian distribution, but from direct measurement of electron energy distribution functions the electron population was found to be non-Maxwellian for regions of the spatial domain inside the discharge chamber.[29,52]

The electron temperature contours in the Figures 12 - 14 illustrate very little variation for the near-DCA probe as the engine is throttled to higher power. There is often a slight discrepancy in the electron temperature between the two interrogation regions, but is within the estimated error due to measurement with different probes. It is very useful to consider two separate investigations to explain the observed electron temperature trends. Analysis of the plasma potentials inside the LM4 discharge illustrate a free-standing double layer aligned with the axial magnetic field near the DCA. The potential gradient structure, termed a double layer, accelerates electrons across the double layer from the discharge cathode plume to the bulk plasma resulting in an increase in the electron temperature. This is supported by analysis of the electron energy distribution functions inside the LM4 discharge chamber.[52] The elevated electron temperature through the double layer is quickly reduced as the higher energy electrons become thermalized. The electron temperature increase near the anode has also been measured near the anode in the discharge channel of Hall thrusters.[53]

The extraction of a beam results in a slight increase in electron temperature, of one or two eV, when compared to data taken without beam extraction. This may be partially due to the increase in discharge voltage associated with beam extraction. The increase in the electron temperatures with beam extraction indicate the coupled nature of the beam and discharge cathodes implying that beam extraction is needed to accurately represent flight-like thruster operating conditions.

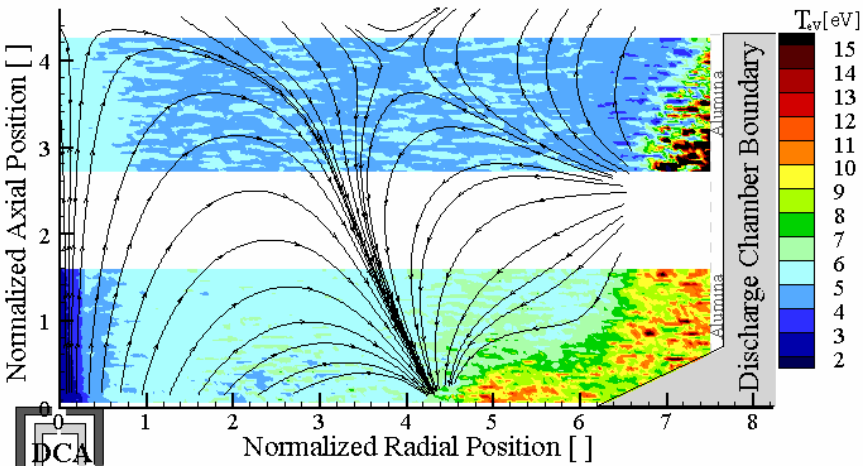

Figure 12: LM4 SLP TOC 0a (V_s = 275V and J_b = 1.00A) electron temperature staggered probe results.

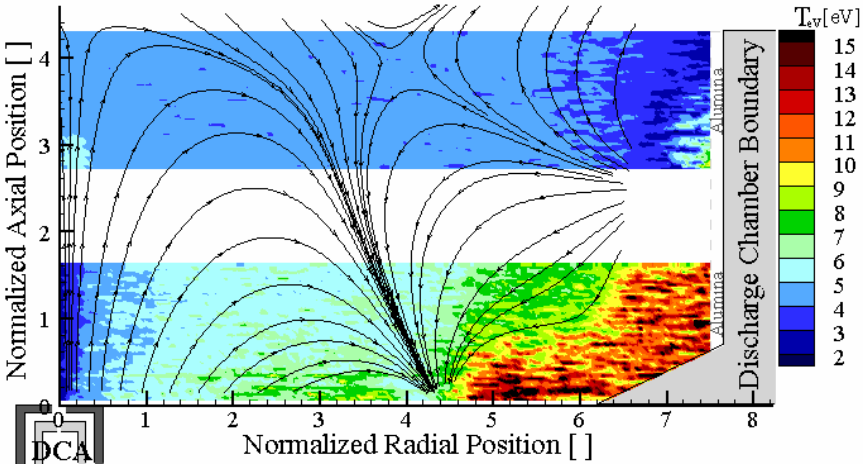

Figure 13: LM4 SLP TOC 8 (V_s = 1179V and J_b = 1.20A) electron temperature staggered probe results.

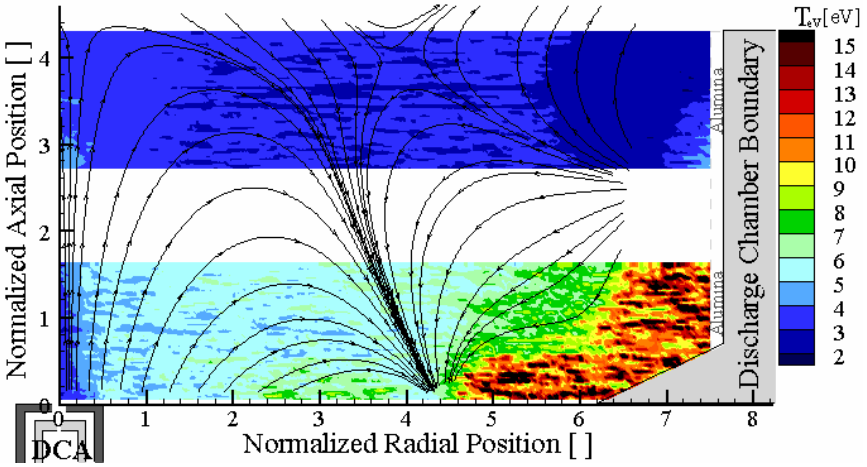

Figure 14: LM4 SLP TOC 34' (V_s = 1459V and J_b = 3.10A) electron temperature staggered probe results.

C. Near-DCA Number Density Measurements

Examination of the near-DCA plasma structure, Figures 15 - 18, is most relevant to the discharge cathode erosion phenomena. This highlights the subtle changes in the discharge cathode plume, the double layer transition, and the overall discharge plasma environment near the DCA. The number density contours from the single Langmuir probe are insensitive to the thruster operating condition in LM4. The axial magnetic field near the DCA creates a distinct plume structure in which cross-field diffusion of electrons is reduced similar to the previous 30-cm NSTAR results.[23,24] However, there is a notable difference between the 30-cm NSTAR FMT2 and 40-cm NEXT LM4 number density plumes. The number density profile for the LM4 exhibits a larger gradient in the axial direction than the FMT2. The decrease in number density in the axial direction for LM4 operation is an order of magnitude at an axial distance of approximately one keeper radius away from the DCA. The axial magnetic field of the LM4 is less than half of the FMT2 thruster at the discharge cathode keeper plate. Therefore, the reduced field of the LM4 does not smooth out the plasma structures in the axial direction the way the FMT2 thruster does. This may significantly affect the DCA erosion mechanisms of the LM4 thruster compared to the FMT2. Number densities at the DCA centerline are as high as $2x10^{13}$ cm^{-3}. Located radially outside the discharge cathode plume (outside the double layer), the plasma number density for the LM4 is ~$5x10^{11}$ cm^{-3}. This value is used to calculate a directed flux of ions, which when combined with plasma potential data, LIF data, and double-to-single ion current ratio yield a calculated NEXT DCA erosion rate.[25,29]

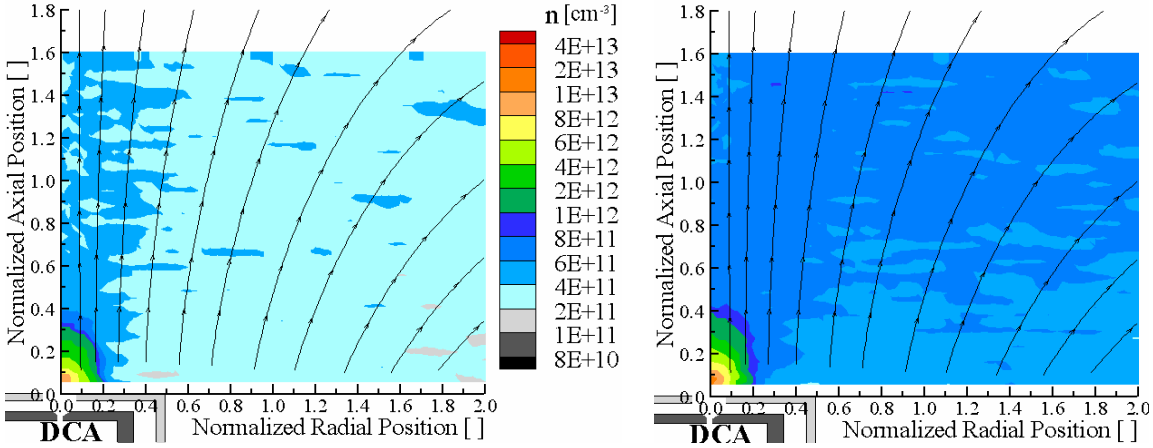

Figure 15: LM4 near-DCA number density contours for SLP TOC 0a - V_s = 275V, J_b = 1.00A (left) and SLP TOC 3 - V_s = 649V, J_b = 1.20A (right).

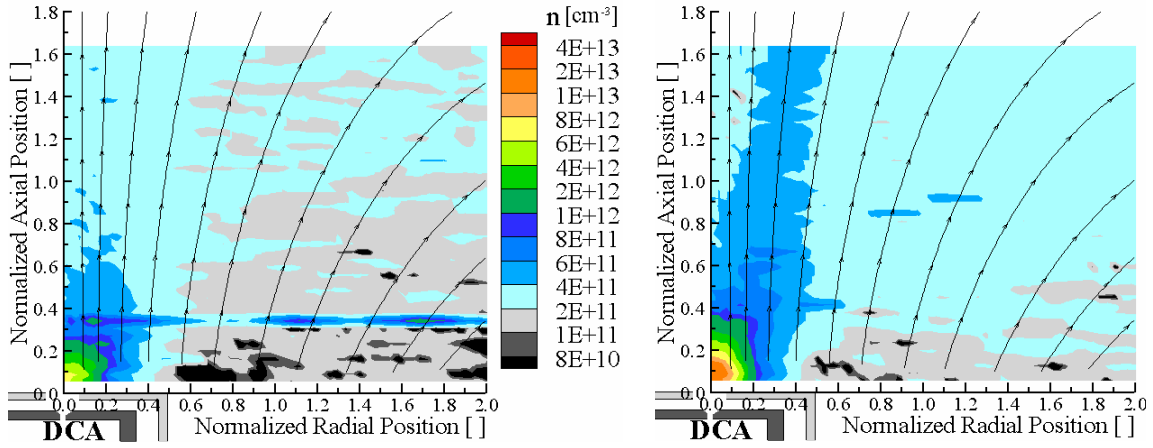

Figure 16: LM4 near-DCA number density contours for SLP TOC 8 - V_s = 1179V, J_b = 1.20A (left) and SLP TOC 18 - V_s = 1179V, J_b = 2.01A (right).

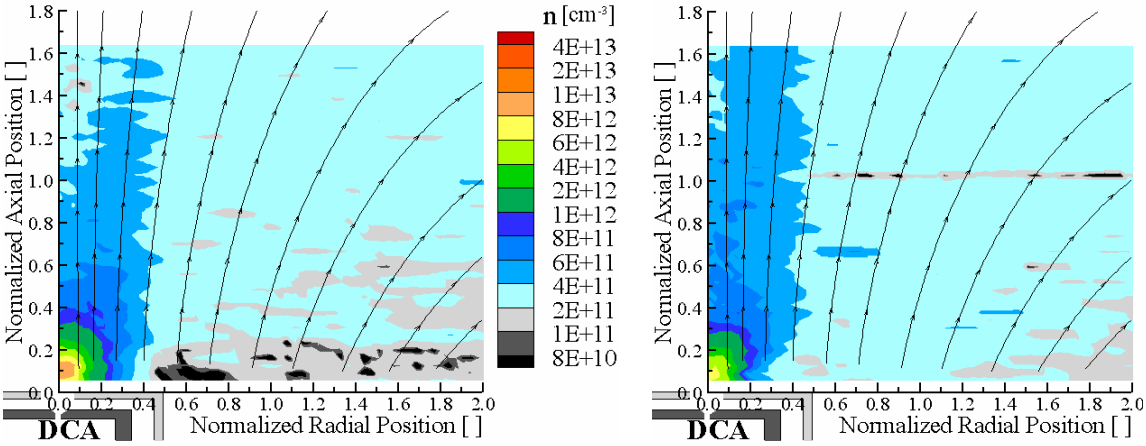

Figure 17: LM4 near-DCA number density contours for SLP TOC 20' - V_s = 1465V, J_b = 2.01A (left) and SLP TOC 32 - V_s = 1179V, J_b = 3.10A (right).

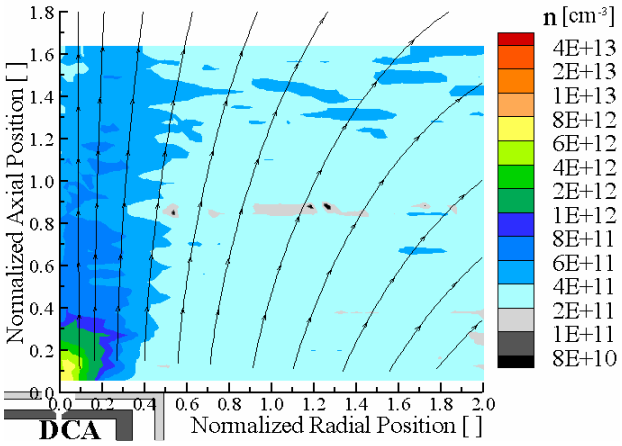

Figure 18: LM4 near-DCA number density contours for SLP TOC 34' - V_s = 1459V, J_b = 3.10A.

D. Near-DCA Electron Temperature Measurements

Near-DCA electron temperatures illustrate a low electron temperature cathode plume with temperatures from 2 – 4 eV inside. Outside the plasma column, the electron temperatures increase up to 4 – 7 eV. The rise in electron temperature is tied to the potential gradients across the boundary between the cathode plume and bulk discharge plasma that accelerates electrons across the boundary thereby increasing their energy. The double layer potential profile also decelerates the high-energy electrons that overcome the potential gradient when moving from the high-potential main discharge plasma to the low-potential cathode plume. This effectively replenishes the low-energy electrons in the discharge cathode plume confirmed in the analysis of the electron energy distribution functions.[52] Very little variation is observed in the near-DCA electron temperatures as the LM4 engine is throttled to higher power in Figures 19 - 22.

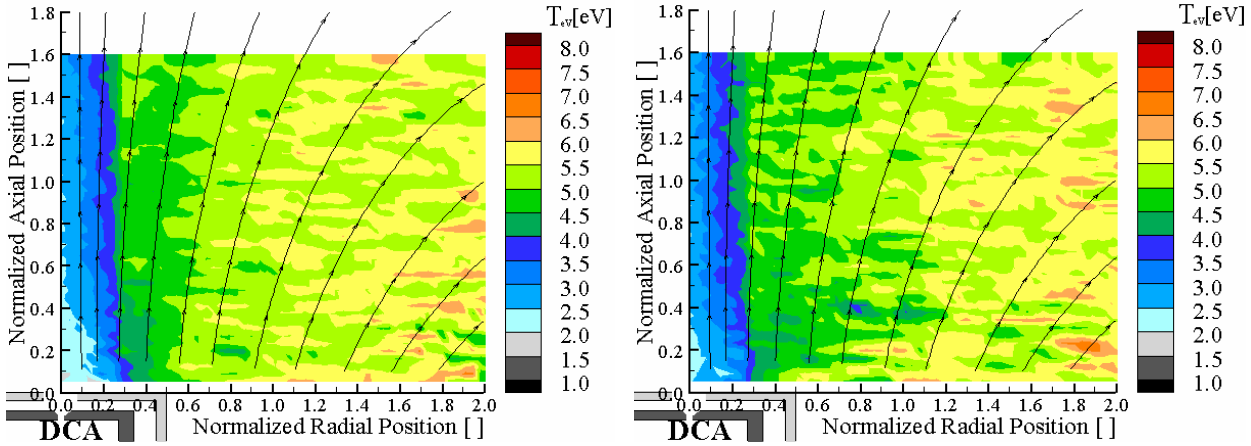

Figure 19: LM4 near-DCA electron temperature contours for SLP TOC 0a - V_s = 275V, J_b = 1.00A (left) and SLP TOC 3 - V_s = 649V, J_b = 1.20A (right).

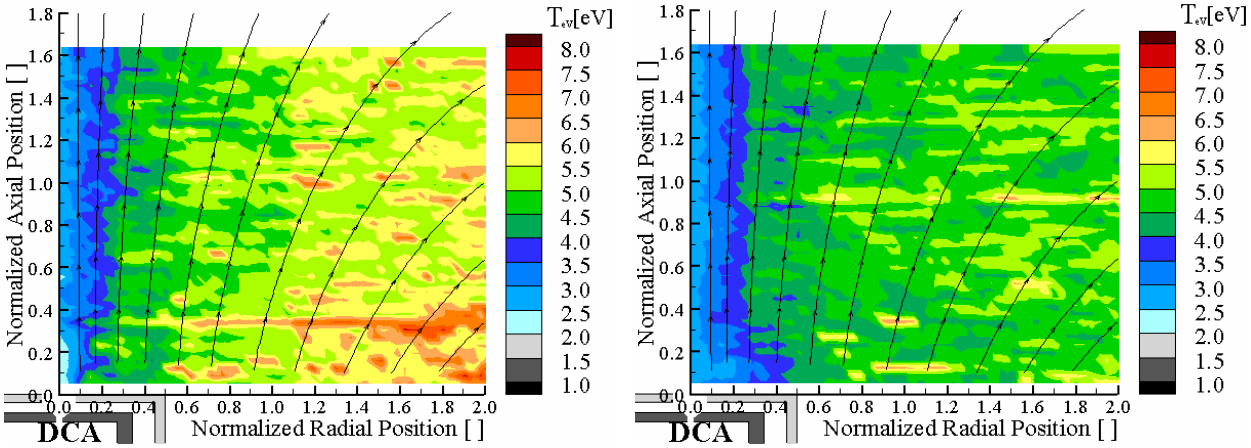

Figure 20: LM4 near-DCA electron temperature contours for SLP TOC 8 - V_s = 1179V, J_b = 1.20A (left) and SLP TOC 18 - V_s = 1179V, J_b = 2.01A (right).

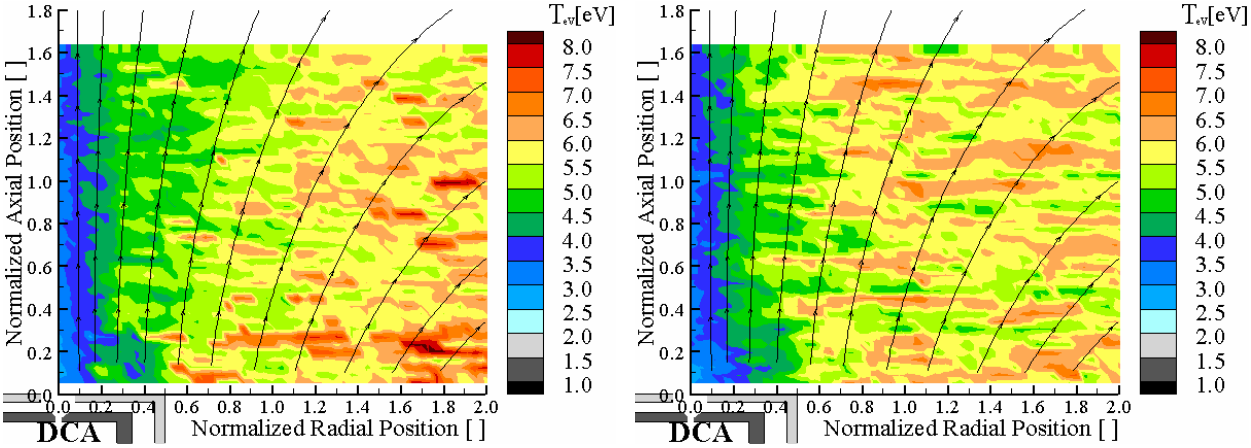

Figure 21: LM4 near-DCA electron temperature contours for SLP TOC 20' - V_s = 1465V, J_b = 2.01A (left) and SLP TOC 32 - V_s = 1179V, J_b = 3.10A (right).

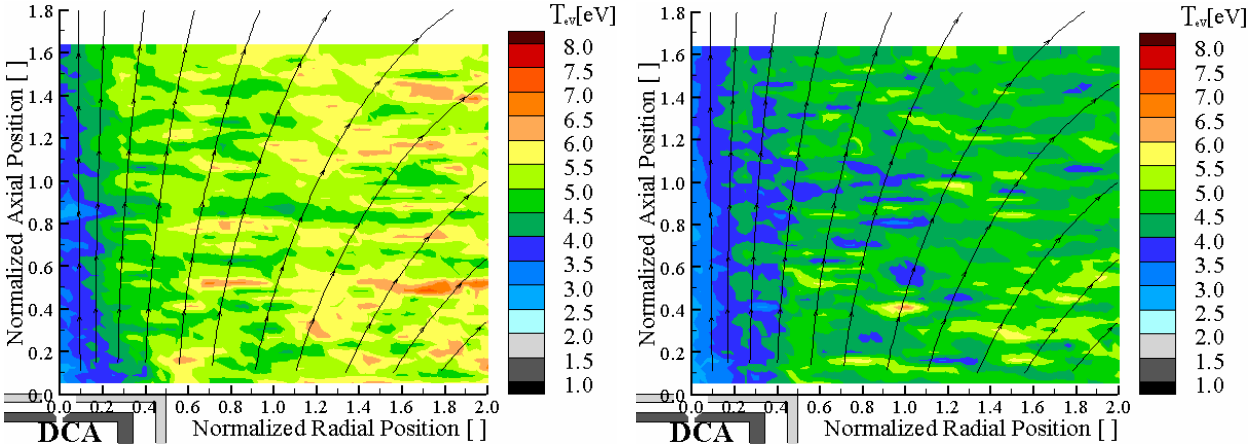

Figure 22: LM4 near-DCA electron temperature contours for SLP TOC 34' - V_s = 1459V, J_b = 3.10A nominal (left) and SLP DL 34' without beam extraction (right).

VI. Discussion

It is evident that the plasma parameter mappings closely follow the magnetic field streamlines. The high-density plume is established by an axial magnetic field near the DCA. As illustrated in plasma potential measurements, the magnetic field that confines the electrons to a narrow plume establishes a free-standing double layer potential gradient. The double layer gradient enhances radial electron motion to offset the magnetic field reduction of radial diffusion by electrostatically accelerating electrons from the DCA plume towards the bulk discharge plasma. This acceleration gives rise to an off-axis increase in electron temperature as electrons are accelerated across the double layer. The double layer also acts to accelerate ions from the bulk discharge plasma towards the DCA giving rise to DCA erosion as outlined in the floating emissive probe investigation on the LM4 thruster.[25,29] The inter-cusp electron temperatures near the anode are extremely high. While this measurement is performed with a poor signal-to-noise ratio it seems logical that only the very high-energy electrons will reach these regions, across magnetic field lines, resulting in an elevated electron temperature.

It is possible that the double layer acceleration of electrons also contributes to ionization in the discharge chamber. Specifically focusing on Figures 16 and 17, there is also an off-axis maximum in number density downstream of the DCA. This may be due to radial acceleration of electrons across the double layer. From emissive probe measurements, the potential across the double layer is approximately 7 volts.[25] Ionization may take place in a step-wise fashion leading to ionization even though the first ionization potential of xenon is 12.13 eV.

Throughout the LM4 investigation, the effects of beam extraction are determined by turning off the high voltage power supplies. Equivalent mass flow rates and discharge currents maintain equivalent number density profiles with and without a beam. The reduction in discharge voltage without a beam decreases the measured plasma potentials inside the discharge chamber. The electron temperatures with beam extraction were slightly higher in magnitude than the discharge-only values illustrated in Figure 22. Examination of the electron energy distribution functions (EEDF's) reveals more broad distributions as the reason for this electron temperature increase (higher-energy electrons are created due to acceleration across the double layer potential gradient). From the LM4 equivalent mass flow approach and the 30-cm NSTAR equivalent discharge voltage approach, it is evident that ion thrusters must be operated at high-voltage to demonstrate equivalent electron temperatures, number densities, and plasma potentials compared to flight conditions.[23,25,29,52,54] All of the discharge plasma parameters are important in describing the discharge plasma environment and therefore the DCA erosion mechanisms. The shorting of the LM4 discharge cathode keeper to cathode common did not have an effect on the discharge plasma outside of the keeper sheath, consistent with the 30-cm NSTAR investigation.

VII. Conclusions

A method of mapping the discharge plasma parameters inside a 40-cm NEXT engine is demonstrated. Number densities are presented for the low to mid-power operation of the LM4 thruster illustrating comparable results to the NSTAR thruster. The number densities illustrate a clear plume structure peaked along centerline (up to $2x10^{13}$ cm^{-3}). The near-DCA centerline value was fairly constant at a value of 1 $x10^{13}$ – $2x10^{13}$ cm^{-3}over the operating conditions investigated. Number densities illustrate negligible dependence upon thruster power level. A number density of ~$5x10^{11}$ cm^{-3} is observed corresponding to a location in the bulk discharge just outside the double layer. This value is utilized to calculate the flux of particles towards the DCA and therefore calculate an erosion rate.

Electron temperatures are similar to those measured in the NSTAR thruster. The electron temperatures in the discharge cathode plume are typically 2 – 4 eV and increase slightly off-axis to 4 – 7 eV. This increase is caused by the acceleration of electrons across the double layer and is confirmed by the electron energy distribution measurements. Outside the off-axis maximum, the electron temperature decreases as the accelerated ions are thermalized. Near the anode wall high electron temperatures are measured. This may be due to sheath formation or double sheath formation on the anode and/or the alumina guiding tube end. This apparent increase in electron temperature near the anode may be enhanced by the decreased signal-to-noise ratio of the measured probe current at these spatial locations.

Acknowledgments

We would like to thank Mr. Michael Patterson of the NASA Glenn Research Center (GRC) for the financial support of this research through research grant NAG3-2216 and for use of government equipment. We would like to acknowledge Dr. John Foster (grant monitor) and Dr. George Williams who have been principal contacts at NASA GRC. We would also like to thank the technicians at NASA GRC, Terry Larrow at the University of Michigan, and Bob Roman who assisted in building the LM4 thruster.

References

[1]Choueiri, E. Y., "A Critical History of Electric Propulsion: The First 50 Years (1906 - 1956)," Journal of Propulsion and Power, Vol. 20, No. 2, pp. 193-203, March-April 2004.

[2]Polk, J. E., Kakuda, R. Y., Anderson, J. R., Brophy, J. R., Rawlin, V. K., Patterson, M. J., Sovey, J. S. and Hamley, J., "Performance of the NSTAR Ion Propulsion System on the Deep Space One Mission," AIAA-2001-0965, *39th AIAA Aerospace Sciences Meeting and Exhibit Joint Propulsion Conference*, Reno, NV, January 8-11, 2001.

[3]Sengupta, A., Brophy, J. R. and Goodfellow, K. D., "Status of the Extended Life Test of the Deep Space 1 Flight Spare Ion Engine after 30,352 Hours of Operation," AIAA-2003-4558, *39th AIAA / ASME / SAE / ASEE Joint Propulsion Conference*, Huntsville, AL, July 20-23, 2003.

[4]Patterson, M. J., Rawlin, V. K., Sovey, J. S., Kussmaul, M. and Parkes, J., "2.3 kW Ion Thruster Wear Test," AIAA-1995-2516, *31st AIAA / ASME / SAE / ASEE Joint Propulsion Conference*, San Diego, CA, July 10-12.

[5]Polk, J. E., Patterson, M. J., Brophy, J. R., Rawlin, V. K., Sovey, J. S., Myers, R. M., Blandino, J. J., Goodfellow, K. D. and Garner, C. E., "A 1000 Hour Wear Test of the NASA NSTAR Ion Thruster," AIAA-1996-2784, *32nd AIAA / ASME / SAE / ASEE Joint Propulsion Conference*, Lake Buena Vista, FL, July 1-3.

[6]Polk, J. E., Anderson, J. R., Brophy, J. R., Rawlin, V. K., Patterson, M. J., Sovey, J. S. and Hamley, J., "An overview of the results from an 8200 hour wear test of the NSTAR ion thruster," AIAA-1999-2446, *35th AIAA / ASME / SAE / ASEE Joint Propulsion Conference*, Los Angeles, California, June 20-24, 1999.

[7]Polk, J. E., Anderson, J. R., Brophy, J. R., Rawlin, V. K., Patterson, M. J. and Sovey, J. S., "The Effect of Engine Wear on Performance in the NSTAR 8000 Hour Ion Engine Endurance Test," AIAA-1997-0869, *33rd AIAA / ASME / SAE / ASEE Joint Propulsion Conference*, Seattle, WA, July 6-9.

[8]Oleson, S.Katz, I., "Electric Propulsion for Project Prometheus," AIAA-2003-5279, *39th AIAA / ASME / SAE / ASEE Joint Propulsion Conference*, Huntsville, AL, July 20-23, 2003.

[9]Oleson, S. R., "Electric Propulsion Technology Development for the Jupiter Icy Moons Orbiter Project," AIAA-2004-3449, *40th AIAA / ASME / SAE / ASEE Joint Propulsion Conference*, Fort Lauderdale, Florida, July 11-14, 2004.

[10]Cupples, M., Coverstone, V. and Woo, B., "Application of Solar Electric Propulsion to a Comet Surface Sample Return Mission," AIAA-2004-3804, *40th AIAA / ASME / SAE / ASEE Joint Propulsion Conference*, Fort Lauderdale, FL, July 11-14.

[11]Oh, D., Benson, S., Witzberger, K. and Cupples, M., "Deep Space Mission Applications for NEXT: NASA's Evolutionary Xenon Thruster," AIAA-2004-3806, *40th AIAA / ASME / SAE / ASEE Joint Propulsion Conference*, Fort Lauderdale, FL, July 11-14.

[12]Benson, S.Patterson, M. J., "Development status of NEXT: NASA's evolutionary xenon thruster," IEPC-03-0288, *28th International Electric Propulsion Conference*, Toulouse, France, March 17-21, 2003.

[13]Williams, G. J., Smith, T. B. and Gallimore, A. D., "30 cm Ion Thruster Discharge Cathode Erosion," IEPC-01-306, *27th International Electric Propulsion Conference*, Pasadena, CA, October 15-19, 2001.

[14]Williams, G. J., Smith, T. B., Patrick, T. A. and Gallimore, A. D., "Characterization of the FMT-2 discharge cathode plume," IEPC-99-104, *26th International Electric Propulsion Conference*, Kitakyushu, Japan, October 1999.
[15]Farnell, C. C., Williams, J. D. and Wilbur, P. J., "Characteristics of energetic ions emitted from hollow cathodes," IEPC-03-072, *28th International Electric Propulsion Conference*, Toulouse, France, March 17-21, 2003.
[16]Foster, J. E.Patterson, M. J., "Plasma emission characteristics from a high current hollow cathode in an ion thruster discharge chamber," AIAA-2002-4102, *38th AIAA / ASME / SAE / ASEE Joint Propulsion Conference*, Indianapolis, IN, July 7-10, 2002.
[17]Foster, J. E.Patterson, M. J., "Characterization of Downstream Ion Energy Distributions from a High Current Hollow Cathode in a Ring Cusp Discharge Chamber," AIAA-2003-4865, *39th AIAA / ASME / SAE / ASEE Joint Propulsion Conference*, Huntsville, AL, July 20-23, 2003.
[18]Foster, J. E., Soulas, G. C. and Patterson, M. J., "Plume and Discharge Plasma Measurements of an NSTAR-type Ion thruster," AIAA-2000-3812, *36th AIAA / ASME / SAE / ASEE Joint Propulsion Conference*, Huntsville, AL., July 16-19, 2000.
[19]Sengupta, A., Goebel, D. M., Fitzgerald, D., Owens, A., Tynan, G. and Doerner, R., "Experimentally Determined Neutral Density and Plasma Parameters in a 30 cm Ion Engine," AIAA-2004-3613, *40th AIAA / ASME / SAE / ASEE Joint Propulsion Conference*, Fort Lauderdale, FL, July 11-14, 2004.
[20]Goebel, D. M., Jameson, K. K., Watkins, R. M. and Katz, I., "Hollow Cathode and Keeper-Region Plasma Measurements using Ultra-Fast Miniature Scanning Probes," AIAA-2004-3430, *40th AIAA / ASME / SAE / ASEE Joint Propulsion Conference*, Fort Lauderdale, FL, July 11-14, 2004.
[21]Herman, D. A.Gallimore, A. D., "A high-speed axial reciprocating probe positioning system for interrogating the discharge plasma of a 30 cm ion thruster," AIAA-2002-4256, *38th AIAA / ASME / SAE / ASEE Joint Propulsion Conference*, Indianapolis, IN, July 7-10, 2002.
[22]Herman, D. A.Gallimore, A. D., "Comparison of Discharge Plasma Parameters in a 30-cm NSTAR Type Ion Engine with and without Beam Extraction," AIAA-2003-5162, *39th AIAA / ASME / SAE / ASEE Joint Propulsion Conference*, Huntsville, Alabama, July 20-23, 2003.
[23]Herman, D. A.Gallimore, A. D., "Near Discharge Cathode Assembly Plasma Potential Measurements in a 30 cm NSTAR-type Ion Engine amidst Beam Extraction," AIAA-2004-3958, *40th AIAA / ASME / SAE / ASEE Joint Propulsion Conference*, Fort Lauderdale, FL, July 11-14.
[24]Herman, D. A., McFarlane, D. S. and Gallimore, A. D., "Discharge plasma parameters of a 30 cm ion thruster measured without beam extraction using a high-speed axial reciprocating probe positioning system," IEPC-03-0069, *28th International Electric Propulsion Conference*, Toulouse, France, March 17-21, 2003.
[25]Herman, D. A.Gallimore, A. D., "Discharge Chamber Plasma Potential Mapping of a 40-cm NEXT-type Ion Engine," AIAA-2005-4251, *41st AIAA / ASME / SAE / ASEE Joint Propulsion Conference*, Tucson, AZ, July 10-13, 2005.
[26]Soulas, G. C., Domonkos, M. T. and Patterson, M. J., "Performance Evaluation of the NEXT Ion Engine," AIAA-2003-5278, *39th AIAA / ASME / SAE / ASEE Joint Propulsion Conference*, Huntsville, AL, July 20-23, 2003.
[27]Soulas, G. C., Kamhawi, H., Patterson, M. J., Britton, M. A. and Frandina, M. M., "NEXT Ion Engine 2000 Hour Wear Test Results," AIAA-2004-3791, *40th AIAA / ASME / SAE / ASEE Joint Propulsion Conference*, Fort Lauderdale, FL, July 11-14.
[28]Hoskins, W. A., Wilson, F. C., Polaha, J., Talerico, L., Patterson, M. J., Soulas, G. C. and Sovey, J. S., "Development of a Prototype Model Ion Thruster for the NEXT System," AIAA-2004-4111, *40th AIAA / ASME / SAE / ASEE Joint Propulsion Conference*, Fort Lauderdale, FL, July 11-14.
[29]Herman, D. A., "The Use of Electrostatic Probes to Characterize the Discharge Plasma Structure and Identify Discharge Cathode Erosion Mechanisms in Ring-Cusp Ion Thrusters," Thesis, Dept. of Aerospace Engineering, University of Michigan, Ann Arbor, MI, 2005.
[30]Haas, J. M., "Low-Perturbation Interrogation of the Internal and Near-field Plasma Structure of a Hall thruster using a High-Speed Probe Positioning System," Ph. D. Thesis, Dept. of Aerospace Engineering, University of Michigan, Ann Arbor, MI, 2001.
[31]Haas, J. M., Gallimore, A. D., McFall, K. and Spanjers, G. G., "Development of a high-speed, reciprocating electrostatic probe system for Hall thruster interrogation," Review of Scientific Instruments, Vol. 71, No. 11, pp. 4131, November 2000.
[32]Haas, J. M.Gallimore, A. D., "Characterization of the internal plasma structure of a 5kw hall thruster," IEPC-99-078, *26th International Electric Propulsion Conference*, Kitakyushu, Japan, October 1999.
[33]Hofer, R. R.Gallimore, A. D., "Recent Results from Internal and Very-Near-Field Plasma Diagnostics of a High Specific Impulse Hall thruster," IEPC-03-037, *28th International Electric Propulsion Conference*, Toulouse, France, March 17-21, 2003.
[34]Williams, G. J., Smith, T. B., Gulczinski, F. S., Beal, B. E., Gallimore, A. D. and Drake, R. P., "Laser Induced Fluorescence Measurement of Ion Velocities in the Plume of a Hall Effect Thruster," AIAA-1999-2424, *35th AIAA / ASME / SAE / ASEE Joint Propulsion Conference*, Los Angeles, CA, June 20-23, 1999.
[35]Williams, G. J., Domonkos, M. T. and Chavez, J. M., "Measurement of doubly charged ions in ion thruster plumes," IEPC-01-310, *27th International Electric Propulsion Conference*, Pasadena, CA, October 15-19, 2001.
[36]Mott-Smith, H. M.Langmuir, I., "The Theory of Collectors in Gaseous Discharges," Physical Review, Vol. 28, pp. 727-763, October, 1926.
[37]Langmuir, I., "The Interaction of Electron and Positive Ion Space Charges in Cathode Sheaths," Physical Review, Vol. 33, pp. 954-989, June 1929.

[38]Beattie, J. R.Matossian, J. N., "Mercury Ion Thruster Technology," NASA CR-174974, Hughes Research Laboratories, 1989.
[39]Domonkos, M. T., "Evaluation of Low-Current Orificed Hollow Cathodes," Ph. D. Thesis, Dept. of Aerospace Engineering, University of Michigan, Ann Arbor, MI, 1999.
[40]Chen, F. F., "Chapter 4: Electric Probes," Plasma Diagnostic Techniques, R. H. Huddlestone and S. L. Leonard, eds., Academic Press, New York,1965.
[41]Chen, F. F., *Introduction to Plasma Physics and Controlled Fusion*, Vol. 1: Plasma Physics, 2nd Ed., Plenum Press, New York, 1984.
[42]Hutchinson, I. H., "Chapter 3: Plasma Particle Flux," Principles of Plasma Diagnostics, Cambridge Universitiy Press, New York,1985.
[43]Chung, P. M., Talbot, L. and Touryan, K. J., "Electric Probes in stationary and flowing plasma: Part 1. Collisionless and transitional probes," AIAA Journal, Vol. 12, No. 2, pp. 133, February 1974.
[44]Schott, L., "Chapter 11: Electrical Probes," Plasma Diagnostics, W. Lochte-Holtgreven, ed., North-Holland Publishing Company, Amsterdam, pp. 668-731,1968.
[45]Ruzic, D. N., *Electric Probes for Low Temperature Plasmas*, The Education Committee American Vacuum Society, New York, 1994.
[46]Hershkowitz, N., "Chapter 3: How Langmuir Probes Work," Plasma Diagnostics, O. Auciello and D. L. Flamm, eds., Academic Press, Inc., Orlando, pp. 113-184,1989.
[47]Mott-Smith, H. M.Langmuir, I., "Langmuir Probe Theory," Physical Review, Vol. 28, pp. 727, 1926.
[48]Chen, F. F., "Langmuir Probe Analysis for High Density Plasmas," Physics of Plasmas, Vol. 8, No. 6, pp. 3029-3041, June 2001.
[49]Passoth, E., Kudrna, P., Csambal, C., Behnke, J. F., Tichy, M. and Helbig, V., "An experimental study of plasma density determination by a cylindrical Langmuir probe at different pressures and magnetic fields in a cylindrical magnetron discharge in heavy rare gases," Journal of Physics D: Applied Physics, Vol. 30, pp. 1763, June 1997.
[50]Aikawa, H., "The Measurement of the Anisotropy of Electron Distribution Function of a Magnetized Plasma," Journal of the Physical Society of Japan, Vol. 40, No. 6, pp. 1741, June 1976.
[51]Sugawara, M., "Electron Probe Current in a Magnetized Plasma," Physics of Fluids, Vol. 9, No. 4, pp. 797-800, April 1966.
[52]Herman, D. A.Gallimore, A. D., "Discharge Cathode Electron Energy Distribution Functions in a 40-cm NEXT-type Ion Engine," AIAA-2005-4252, *41st AIAA / ASME / SAE / ASEE Joint Propulsion Conference*, Tucson, AZ, July 10-13, 2005.
[53]Dorf, L., Raitses, Y. and Fisch, N. J., "Experimental studies of anode sheath phenomena in a Hall thruster discharge," Journal of Applied Physics, Vol. 97, May 2005.
[54]Herman, D. A.Gallimore, A. D., "Discharge Chamber Plasma Structure of a 40-cm NEXT-type Ion Engine," AIAA-2005-4250, *41st AIAA / ASME / SAE / ASEE Joint Propulsion Conference*, Tucson, AZ, July 10-13, 2005.